



1 **Austral Summer MJO Forecast Skill in S2S Models: Decadal Shifts and Their Drivers**

2 Raina Roy ^{a,b*}, Julie M. Arblaster ^{a,b}, Matthew C. Wheeler ^c, Eun-Pa Lim ^c, Jadwiga. H. Richter ^d

3

4 ^aSecuring Antarctica's Environmental Future, Monash University, Clayton, VIC, Australia

5 ^bSchool of Earth, Atmosphere and Environment, Monash University, Clayton, VIC, Australia.

6 ^cResearch, Bureau of Meteorology, Melbourne, VIC, Australia.

7 ^dNational Center for Atmospheric Research, Boulder, Colorado, USA

8

9

10

11

12

13

14

15

16

17

18

19

20

21

22

23

24

25

26

27

28

29

30

31

32

33



34 * To whom **correspondence** should be addressed. Email: raina.roy@monash.edu

35

36 **Short title: Decadal Variability in MJO Forecast Skill**

37

38 **Keywords: MJO, Prediction Skill, S2S Forecasts, QBO, IOD, ENSO, IOBM**

39 **ADDRESS FOR COMMUNICATIONS**

40

41

42

43

44

45

46

47

48

49

50

51

52

53

54

55



56 **Highlights**

- 57 • The MJO exhibits greater inherent predictability in 1981-1998 compared to 1999-
58 2018, primarily due to stronger MJO amplitude (higher signal-to-noise ratio).
59 • Climate forcings (QBO, IOD, ENSO) play a primary role in modulating MJO skill in the
60 models, overcoming model mean state biases.
61 • Peak skill in MJO prediction is found when easterly QBO (EQBO) winds coincide with
62 negative IOD or La Niña, a synergy that weakened after 1998.
- 63
64
65
66
67
68
69
70
71
72
73
74
75
76
77
78
79
80
81
82
83
84
85
86
87
88
89
90
91
92
93
94
95
96
97
98
99
100
101
102
103



Abstract

The Madden–Julian Oscillation (MJO) is a key driver of global subseasonal-to-seasonal (S2S) climate variability, initiating teleconnections that affect weather patterns worldwide. Improving understanding of the factors that constrain MJO predictability is therefore critical for advancing S2S forecasting systems. Using a multi-model framework, we evaluate changes in MJO prediction skill between two periods (1981–1998 and 1999–2018) during austral summer (December–February) and examine the processes underpinning these differences. Our analysis reveals a pronounced decadal decline in MJO forecast skill, with high-skill years in 1981–1998 showing prediction lead times of around 10 days longer (based on the bivariate correlation of the Real-Time Multivariate MJO (RMM) index) than in 1999–2018, while low-skill years show little change. This asymmetric reduction coincides with stronger MJO amplitude in the earlier period, despite relatively stable model mean-state biases in tropical sea surface temperatures (SSTs) and lower-tropospheric moisture. Key findings include: (1) persistent moisture biases across both periods, yet higher skill in 1981–1998, suggesting that model errors alone cannot explain the differences; (2) a stronger Quasi-Biennial Oscillation (QBO)–MJO relationship in the first period, independent of stratospheric resolution in the models; and (3) weakened coupling between the MJO and large-scale climate modes, including the QBO, El Niño–Southern Oscillation (ENSO), and Indian Ocean Dipole (IOD), in 1999–2018, indicating reduced dynamical support for prediction. These results suggest that decadal variations in MJO skill are strongly influenced by changes in the background dynamical environment. They highlight the need for S2S systems to improve representation of tropospheric processes and stratosphere–troposphere coupling, particularly when large-scale climate forcing is weak.



146

147 **1. Introduction**

148 The Madden-Julian Oscillation (MJO), first identified by Madden and Julian (1971, 1972), is
149 the dominant mode of intraseasonal tropical climate variability. Through its planetary-scale
150 coupling of convection and circulation, the MJO modulates global weather systems via
151 teleconnections and directly influences monsoons, extreme events, and extratropical
152 patterns (Tseng et al., 2018; Lim et al., 2021a; Stan et al., 2022; Roy et al., 2025). These far-
153 reaching impacts make MJO prediction vital for subseasonal-to-seasonal (S2S) forecasting
154 (Zhang, 2013; Jiang et al., 2020). Despite its critical role in S2S predictability, accurately
155 forecasting the MJO remains a persistent challenge for state-of-the-art dynamical models
156 (Kim et al., 2019a). Since the landmark Intraseasonal Variability Hindcast Experiment (ISVHE)
157 in 2014, coordinated multi-model efforts have systematically advanced MJO prediction
158 capabilities through improved model physics, initialisation, and ensemble strategies (Neena
159 et al., 2014; Vitart, 2017; Pegion et al., 2019). These advances have extended MJO prediction
160 skill to approximately 25-30 days in leading systems (Kim et al., 2019a).

161

162 Despite modelling improvements, persistent deficiencies in simulating MJO propagation
163 across the Maritime Continent (MC) continue to limit prediction skill, particularly for MC-
164 terminating events compared to those propagating beyond (Abhik et al., 2023). This
165 persistent "MC barrier effect" (Zhang & Ling, 2017) arises primarily from model deficiencies
166 in representing the region's complex orography, diurnal precipitation cycles, and lower-
167 tropospheric moisture preconditioning (e.g., Peatman et al., 2014; Gonzalez & Jiang, 2017;
168 Ling et al., 2019; Savarin & Chen, 2023). These issues are compounded by systematic mean
169 state biases throughout the tropical Indo-Pacific, including an overly dry lower troposphere
170 and erroneous circulation patterns over the MC region (Kim et al., 2019a; Zavadoff et al.,
171 2023). Furthermore, MJO prediction skill exhibits strong sensitivity to initial conditions, with
172 forecast reliability depending on the event's initial amplitude and genesis location,
173 particularly for Indian Ocean-initiated events (Rashid et al., 2011; Lim et al., 2018; Wu et al.,
174 2023).

175

176 While these tropospheric factors dominate MJO predictability and representation in models
177 (e.g., Kim et al., 2014; Lin et al., 2024), stratospheric influences also play a critical role. In
178 particular, the Quasi-Biennial Oscillation (QBO) modulates MJO amplitude and propagation
179 through stratosphere–troposphere interactions (Son et al., 2017; Nishimoto & Yonden, 2017).
180 This modulation also extends MJO forecast skill, with S2S models consistently showing higher
181 predictability during the easterly QBO (EQBO) phases, when equatorial stratospheric winds
182 blow from east to west (Abhik & Hendon, 2019). The physical mechanisms underlying this
183 modulation involve two key processes: (1) EQBO-induced cold anomalies in the upper
184 troposphere-lower stratosphere (UTLS) that reduce static stability and promote deep
185 convection, and (2) more effective cloud-radiative feedback that amplifies and sustains MJO
186 circulation (Marshall et al., 2017; Hendon & Abhik, 2018; Sakaeda et al., 2020; Jin et al., 2023).
187 Notably, the observed QBO-MJO relationship has intensified in recent decades, likely linked
188 to stratospheric cooling and tropospheric warming trends (Klotzbach et al., 2019). Despite
189 this well-documented connection, most global forecast models struggle to replicate the QBO-
190 MJO relationship (e.g., Kim et al., 2019b; Martin et al., 2021). Kim et al. (2019b) demonstrated



191 only a weak QBO-MJO relationship reproduced by most forecast systems during the 1999-
192 2015 period.

193

194 While the QBO's role in MJO predictability is well established, the impacts of tropical sea
195 surface temperature (SST) variability remain less understood and appear to be model-
196 dependent. Zhou et al. (2024) recently identified enhanced MJO prediction skill during boreal
197 winter basin-wide warm Indian Ocean SST events, mediated through intensified convective
198 instability. However, their analysis was restricted to model simulations from the post-1999
199 period. This finding suggests a potentially essential but underexplored connection between
200 the Indian Ocean Basin Mode (IOBM) and MJO predictability, consistent with known
201 thermodynamic controls on MJO propagation.

202

203 Similarly, Liu et al. (2017) demonstrated that Indian Ocean variability (particularly positive
204 Indian Ocean Dipole phases) might govern the upper limit of MJO predictability in the forecast
205 system. However, they cautioned about the potential model overestimation of this
206 relationship. Notably, both analyses were restricted to shorter periods (about ~ 20 years),
207 leaving open questions about the robustness of these relationships across different climate
208 states and longer timescales. The El Niño Southern Oscillation (ENSO)-MJO relationship
209 exhibits particular complexity, with studies reporting improved skill during both El Niño (via
210 strengthened air-sea coupling; DeMott et al., 2018; Wu et al., 2023) and La Niña conditions
211 (Kim et al., 2018; Mengist & Seo, 2022). This suggests that oceanic mode-MJO relationships
212 are non-stationary, likely reflecting their sensitivity to evolving background climate states on
213 decadal timescales (Zhao et al, 2016).

214 This study addresses these knowledge gaps through a multi-model framework examining
215 decadal shifts in MJO predictability during boreal winter/austral summer (December–
216 February (DJF))—the season of peak MJO activity and strongest coupling with major climate
217 modes (ENSO, QBO, IOD, IOBM). Using four S2S hindcast datasets, together with
218 observational verification and statistical benchmarking, we:

- 219 1. disentangle intrinsic MJO predictability from model-specific biases;
- 220 2. quantify how the influence of large-scale climate modes on predictability varies
221 between 1981–1998 and 1999–2018; and
- 222 3. diagnose the role of evolving background states in shaping the mechanisms and
223 thresholds of MJO predictability.

224

225 For the rest of the paper, we will describe forecast model configurations, forecast and
226 verification data, and analysis methods in Section 2 and present results with discussion
227 in Section 3. Then, we will provide concluding remarks in Section 4.

228 **2. Data and Methods**

229 **2.1 Datasets**

230 This study analyses four independent subseasonal-to-seasonal (S2S) hindcast datasets to
231 evaluate MJO prediction skills across different modelling systems: the Predictive Ocean-
232 Atmosphere Model for Australia Version 2 (POAMA2, Cottrill et al. 2013), the Australian



233 Community Climate and Earth-System Simulator—Seasonal (ACCESS-S2, Wedd et al., 2022),
234 the Community Earth System Model Version 2 (CESM2, Richter et al., 2022), and the Global
235 Earth Observing System S2S model Version 2 (GEOS-S2S-2, Molod et al., 2020). These models
236 were selected from the wider S2S database based on the availability of sufficiently long
237 hindcasts, ensemble sizes, and initialisation frequencies to permit robust skill assessment. In
238 particular, POAMA2 and ACCESS-S2 provide extended archives (1981–2018), forming the core
239 of our decadal comparison, while CESM2 and GEOS-S2S-2, available for the later period
240 (1999–2018), are incorporated to broaden the analysis to more recent state-of-the-art
241 systems and to test the robustness of the identified mechanisms across diverse model
242 configurations.

243 Key features of each hindcast—including vertical resolutions, ensemble sizes, initialisation
244 frequencies, and hindcast durations—are summarised in Table 1. The study employs three
245 primary observational datasets for verification: (1) NCEP/DOE Reanalysis II (NCEP2) for
246 atmospheric variables (Kanamitsu et al., 2002), (2) NOAA AVHRR Outgoing Longwave
247 Radiation (OLR) as a proxy for tropical convection (Liebmann & Smith, 1996), and (3) the
248 NOAA OISST V2 SST dataset (Huang et al., 2021). These datasets span the 1981–2018 study
249 period and were regridded to a consistent $2.5^\circ \times 2.5^\circ$ global grid to facilitate comparison with
250 model outputs. All model hindcasts (POAMA2, ACCESS-S2, CESM2, GEOS-S2S-2) are regridded
251 to match the observational $2.5^\circ \times 2.5^\circ$ grid.

252 2.1.2 Climate Indices

253 MJO activity is quantified using the Real-Time Multivariate MJO (RMM) index (Wheeler &
254 Hendon, 2004), which is derived from the combined anomalies of OLR and zonal winds at 200
255 hPa and 850 hPa. For climate mode classification, ENSO phases are identified using the Niño
256 3.4 index (Trenberth, 1997), with El Niño (La Niña) defined when the 5-month running mean
257 of SST anomalies in the Niño 3.4 region (5°S – 5°N , 170° – 120°W) exceeds $+0.5\sigma$ (falls below
258 -0.5σ). The running mean is applied continuously throughout the year, ensuring that phase
259 classification captures the persistence of ENSO anomalies relevant to the DJF period under
260 analysis. IOD events are tracked using the Dipole Mode Index (DMI) (Saji et al., 1999), which
261 is calculated as the difference in SST anomalies between the tropical western (50° – 70°E , 10°S –
262 10°N) and eastern (90° – 110°E , equator– 10°S) Indian Ocean (i.e., the western pole minus the
263 eastern pole). Events are classified as positive or negative IOD based on the DJF mean of the
264 DMI. A positive IOD event is defined when the DJF-averaged DMI exceeds $+0.5\sigma$ (relative to
265 the DJF climatology), and a negative IOD when it falls below -0.5σ . The Indian Ocean Basin
266 Mode (IOBM) index is computed as the area-weighted average of SST anomalies across the
267 tropical Indian Ocean (20°S – 20°N , 40° – 110°E), following Xie et al. (2009). Warm (cold) IOBM
268 events are identified when the standardised index exceeds $+0.5\sigma$ (falls below -0.5σ). QBO
269 phases are determined using 50 hPa zonal wind anomalies averaged over 5°S – 5°N (U50) from
270 NCEP2, with easterly (westerly) phases defined as $U50 < -0.5\sigma$ ($U50 > +0.5\sigma$) (Son et al., 2017).



Model	Pressure levels (hPa)	Temporal Range	Ensemble Members	Initialization Frequency (Days of the Month)	References
POAMA2 (Low top model)	17 Levels (model top at 9 hPa)	1981-2018	11	01,06,16,26	Cottrill et al. (2013)
ACCESS-S2 (high-top model)	85 levels (model top at ~ 0.01 hPa)	1981-2018	3	01,06,16,26	Wedd et al. (2022)
CESM2 (Low top model)	32 vertical levels (model top at 2.26 hPa)	1999-2018	11	1/week	Richter et al. (2022)
GEOS-S2S-2 (high-top model)	72 vertical levels (model top at 0.01hPa)	1999-2018 (data unavailable for early 2017)	4	1/week	Molod et al. (2020) Lim et al. (2021b)

Table 1. Summary of S2S hindcast datasets analysed in this study

To evaluate MJO prediction skill, we compare dynamical model forecasts against both observations and predictions from the Vector Autoregression (VAR) model developed by Maharaj & Wheeler (2005). This statistical approach serves as a key benchmark for assessing the performance of dynamical models, as established in previous studies (Rashid et al., 2011). The VAR model predicts MJO evolution using initial values of the RMM indices (RMM1 and RMM2) along with their lagged temporal variations, effectively functioning as an advanced bivariate persistence forecast. Further details of the VAR model's mathematical formulation and training procedures are provided in Marshall et al. (2016). This statistical benchmark enables systematic evaluation of whether dynamical models outperform a simple empirical statistical model. This study employs a period-stratified approach, analysing all observational data, dynamical model outputs (POAMA2, ACCESS-S2, CESM2, GEOS-S2S-2), and statistical benchmarks exclusively within two independent periods (1981–1998 and 1999–2018) to address potential non-stationarities in MJO behaviour. The VAR model is separately calibrated for each period through distinct regression coefficients (see supplementary text). By maintaining identical period divisions across all components (models, observations, and VAR), we control for background state variability and accurately quantify the evolution of skill across different periods.



2.2 Methods

Our analysis employs bivariate correlation (B.Corr) between observed and forecasted MJO RMM indices (Rashid et al., 2011) to quantify MJO prediction skill during austral summer (DJF), focusing specifically on the subseasonal window (15–25-day leads) where operational forecasting transitions from weather to climate timescales (see supplementary text). This subseasonal window is used to compute an interannually varying skill index. A 15–25-day window to calculate the skill index is selected for two key reasons:

1. Subseasonal Focus: This window captures the critical transition period where deterministic weather forecasts lose skill, but MJO predictability remains viable, addressing the core S2S prediction challenge.
2. Signal clarity: In this range, interannual variations in MJO prediction skill are physically coherent and consistent across models, unlike at shorter leads (dominated by initial conditions) or longer leads (where noise overwhelms the signal). Broader windows (e.g., 10–30 days) were also tested, but these either biased the index toward initial-condition dependence or introduced substantial noise, reducing cross-model consistency.

To examine decadal changes in MJO predictability, we classified years into high- versus low-skill categories for each of ACCESS-S2, POAMA-2, CESM2, GEOS-S2S-2 and for 1981-1998 (ACCESS-S2 and POAMA2 only) and 1999-2018 using the 15–25-day bivariate correlation MJO skill index (see supplementary text for detailed methodology). We identified the top seven highest-scoring years as "Good MJO prediction years" (high-skill) and the bottom seven years as "Poor MJO prediction years" (low-skill) for each model-period combination. This comparison approach provides maximum diagnostic contrast between high- and low-skill regimes, allowing us to isolate the specific climate conditions (e.g., ENSO, QBO, IOD phases) and model characteristics that enhance or degrade MJO forecast skill. Selecting seven years per category corresponds to approximately the top and bottom 40% of cases in each period, providing a balance between statistical robustness and clear separation of skill levels.

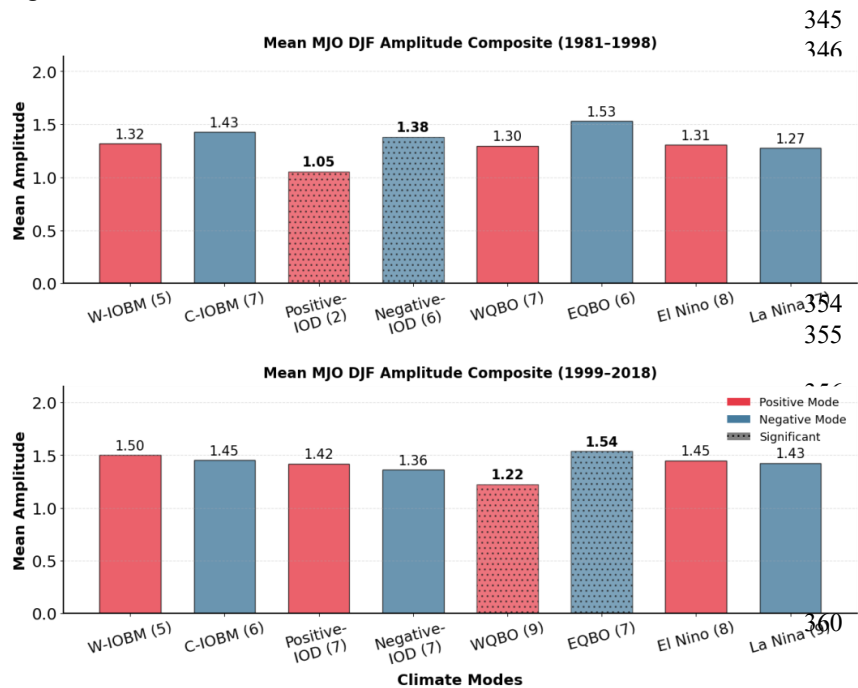
To investigate drivers of MJO predictability, we correlate each model's MJO skill index with key climate indices: Niño 3.4 (ENSO), Zonal wind anomalies at 50 hPa (QBO), DMI (IOD), and the IOBM Index. The climate indices are derived from observed datasets. The MJO amplitude and phase are derived following Rashid et al. (2011), ensuring compatibility with established verification frameworks. We detect and track MJO events using a modified version of the Wei and Ren (2019) methodology. While their original approach focused solely on Indian Ocean-initiated events, our implementation extends coverage to all MJO phases (1-8). This adaptation provides three advantages: (1) it captures the full spectrum of observed MJO behaviour, including Pacific-originating events; (2) it eliminates geographical selection biases that could skew model verification; and (3) it increases the sample size of detectable events, enhancing statistical robustness. Steps to classify MJO events are discussed in detail in the supplementary text. We also employ linear regression between the MJO skill indices and key variables (OLR and 850 hPa specific humidity anomalies) for both observations and model forecasts to examine the background state changes associated with high MJO skill years versus low MJO skill years. Observational data are restructured to match forecast conventions, with four monthly start dates and MJO evolution time is calculated accordingly, ensuring consistent comparison with model outputs.



333 **3. Results and Discussions**

334 **3.1 Observed MJO characteristics**

335 Figure 1 highlights apparent epochal differences in the modulation of observed MJO
336 amplitude by key climate modes. During the earlier period (1981–1998; Fig. 1, top row), MJO
337 amplitude is significantly higher during (1) negative Indian Ocean Dipole (N-IOD) compared to
338 positive IOD, and (2) easterly Quasi-Biennial Oscillation (EQBO) compared to westerly QBO,
339 as indicated by stippling. Amplitude is also higher during cold Indian Ocean Basin Mode (C-
340 IOBM) years, although this difference is not statistically significant. In contrast, during the
341 later period (1999–2018; Fig. 1, bottom row), these phase-dependent relationships undergo
342 a marked reorganisation: the EQBO–MJO linkage strengthens, while the previously significant
343 IOD contrast weakens and falls below statistical significance, and C-IOBM differences remain
344 non-significant.



361 **Figure 1:** Composite mean amplitude of the MJO across different phases of climate indices—
362 IOBM, IOD, QBO, and Niño 3.4—during austral summer. The top row displays results for the
363 period 1981–1998, while the bottom row shows the same for 1999–2018. Numbers in
364 parentheses denote the number of years included in each composite phase. The statistical
365 significance of MJO amplitude differences between positive and negative phases of each
366 index was assessed using a bootstrapping approach (10,000 iterations), where years were
367 randomly resampled (7 per phase). Hatched bars/bold text above the bars indicate
368 differences exceeding the 90th percentile confidence threshold.

369 In the earlier epoch, enhanced MJO amplitude during specific IOD and IOBM years may be
370 partly associated with concurrent EQBO conditions. Moderate correlations between the QBO



371 and IOD ($r = 0.32$) and IOBM ($r = 0.34$) indices suggest some co-variability between
372 stratospheric and Indian Ocean conditions. Notably, IOD and IOBM are significantly correlated
373 ($r = 0.39$), indicating shared variability between these two Indian Ocean modes, while a
374 weaker correlation exists between QBO and ENSO ($r = 0.19$). Together, these associations
375 imply that MJO amplitude during this period was likely influenced by a combination of
376 stratospheric (QBO) and tropospheric (Indian and Pacific Ocean SST) factors.

377 While previous studies (e.g., Sun et al., 2019; Mengist & Seo, 2022; Takasuka et al., 2025) have
378 emphasised the role of EQBO–La Niña co-occurrence in enhancing MJO convection and
379 reducing the blocking effect of the Maritime Continent, it is notable that La Niña events
380 frequently coincide with negative IOD- and IOBM-like states (Schott et al., 2009; Cai et al.,
381 2011; Lim et al., 2017). The negative phase of the IOD, characterised by enhanced low-level
382 moisture and reduced atmospheric stability over the eastern Indian Ocean (Kug et al., 2009;
383 Wilson et al., 2013), provides a thermodynamic environment favourable for MJO
384 development, particularly in phases 1 and 2. Similarly, the cold phase of the IOBM, associated
385 with basin-wide SST cooling, can promote increased atmospheric instability and moisture
386 convergence across the Indian Ocean sector, particularly in phases 3 and 4. These conditions
387 likely acted in concert with EQBO to strengthen MJO amplitude during the 1981–1998 period,
388 highlighting a synergistic interaction between stratospheric and tropospheric drivers.

389 In contrast, the 1999–2018 period exhibited intensified EQBO–MJO coupling (Klotzbach et al.,
390 2019) but a breakdown of tropospheric linkages, with QBO–IOD/IOBM correlations
391 weakening to $r = 0.15$ – 0.13 and QBO–ENSO becoming slightly anti-correlated ($r = -0.18$). This
392 breakdown reflects a fundamental shift in the background state, where the loss of combined
393 stratospheric-tropospheric forcing—exacerbated by a weakened N-IOD–La Niña relationship
394 post-1999 (Zu et al., 2024)—diminished MJO amplitude modulation.

395 To further characterise MJO variability, we examined relationships between interannual MJO
396 event properties (mean DJF duration and total yearly event count for DJF) and climate mode
397 indices. The QBO exerted the most substantial and most persistent influence, with MJO event
398 duration showing robust negative correlations (1981–1998: $r = -0.67$; 1999–2018: $r = -0.50$).
399 Composite analysis (Figure S1) illustrates the frequency distribution of MJO phases, showing
400 that in EQBO years, particularly during 1981–1998, the MJO spends more days in phases 3–6.
401 Although the figure does not directly plot event duration, this higher phase occupancy reflects
402 longer-lived events, consistent with the negative correlation between QBO and mean DJF
403 event duration ($r = -0.67$). In contrast, MJO event count exhibited weaker associations with
404 QBO ($r = -0.28$ to -0.20).

405 The tropospheric modes exhibited temporally varying relationships with MJO frequency: (1)
406 the DMI correlated negatively with event count in 1981–1998 ($r = -0.48$, reflecting enhanced
407 frequency during N-IOD years), but this relationship reversed sign and weakened post-1998;
408 (2) the IOBM index developed a positive correlation ($r = 0.38$) in the later period (more events
409 during W-IOBM years); and (3) ENSO (Niño 3.4) showed strong positive correlations in the
410 first period ($r = 0.46$, linking El Niño (La Niña) to increased (decreased) MJO activity) that
411 weakened substantially thereafter. This weakening of tropospheric mode relationships in the
412 second period may stem from reduced co-occurrence of favourable QBO and tropospheric
413 climate mode phases. Notably, none of the tropospheric indices (IOD, IOBM, ENSO)
414 significantly correlated with MJO duration, underscoring that while they modulate initiation



frequency, event longevity is governed primarily by stratospheric (QBO) processes. Figure S1 composites illustrate these dynamics: EQBO years in 1981–1998 featured both greater total MJO days and more substantial phase-specific enhancement (phases 3–6), whereas tropospheric influences (e.g., El Niño/N-IOD/W-IOBM linkages to MJO frequency) weakened or reversed in the later period. Collectively, these results demonstrate a stark contrast: tropospheric mode relationships with MJO evolved markedly between periods, while the QBO’s stratospheric influence remained robust, highlighting its dominant role in MJO prediction.

3.2 MJO skill indices in the models

As found in previous studies, all dynamical models exhibit appreciable skill for the 15–25 day lead time during most years, with bivariate correlations generally above ~0.5, indicating meaningful predictability of the MJO at subseasonal timescales. Figure 2 reveals systematic differences in MJO forecast skill between models and across the two periods. Dynamical models show strong inter-model agreement in skill indices during both 1981–1998 (Fig. 2A) and 1999–2018 (Fig. 2B), while the statistical VAR model (yellow line) consistently underperforms - a pattern confirmed also by the mean skill comparison with lead time (Fig. 2C, yellow line). POAMA2 emerges as the highest-skill dynamical model (green solid line; ~26-day skill) (Fig. 2C), potentially attributable to its enhanced MJO amplitude relative to observations (compare green and black solid lines; Fig. 2D). It is also noteworthy that the MJO amplitude is substantially underestimated in ACCESS-S2 (blue lines), particularly during the second period, compared to the other models and observations. This amplitude deficiency, however, does not translate to proportionally reduced forecast skill; the model maintains skill levels comparable to those of other dynamical models for this period. This apparent discrepancy suggests that while accurate amplitude representation may contribute to forecast skill (as seen in POAMA2’s strong first-period performance), other factors may play compensatory roles in maintaining usable skill despite amplitude biases in ACCESS-S2.

A comparison of good MJO prediction years reveals substantial differences between periods (Fig. 2E, compare the solid and dashed lines). ACCESS-S2 and POAMA2 demonstrate approximately 10 days greater forecast skill during 1981–1998 compared to 1999–2018, with this enhancement directly attributable to stronger MJO amplitudes in the earlier period (Fig. 2F, compare solid and dashed lines). The statistical VAR model shows a similar, though statistically insignificant ($p > 0.05$), first-period skill advantage. In contrast, the skill difference between the first and second periods disappears in years with poor MJO predictions (Fig. 2G, compare solid and dashed lines), where all models exhibit comparable performance across periods. Importantly, there is strong consistency across models in the classification of good- and poor-prediction years, with most years falling into the same category across systems, reinforcing the robustness of the inter-model signal. These results suggest that recent changes in tropical climate dynamics—such as changes in the background state—have disproportionately affected MJO prediction skill in good MJO prediction years, while leaving poor-prediction years relatively unchanged.

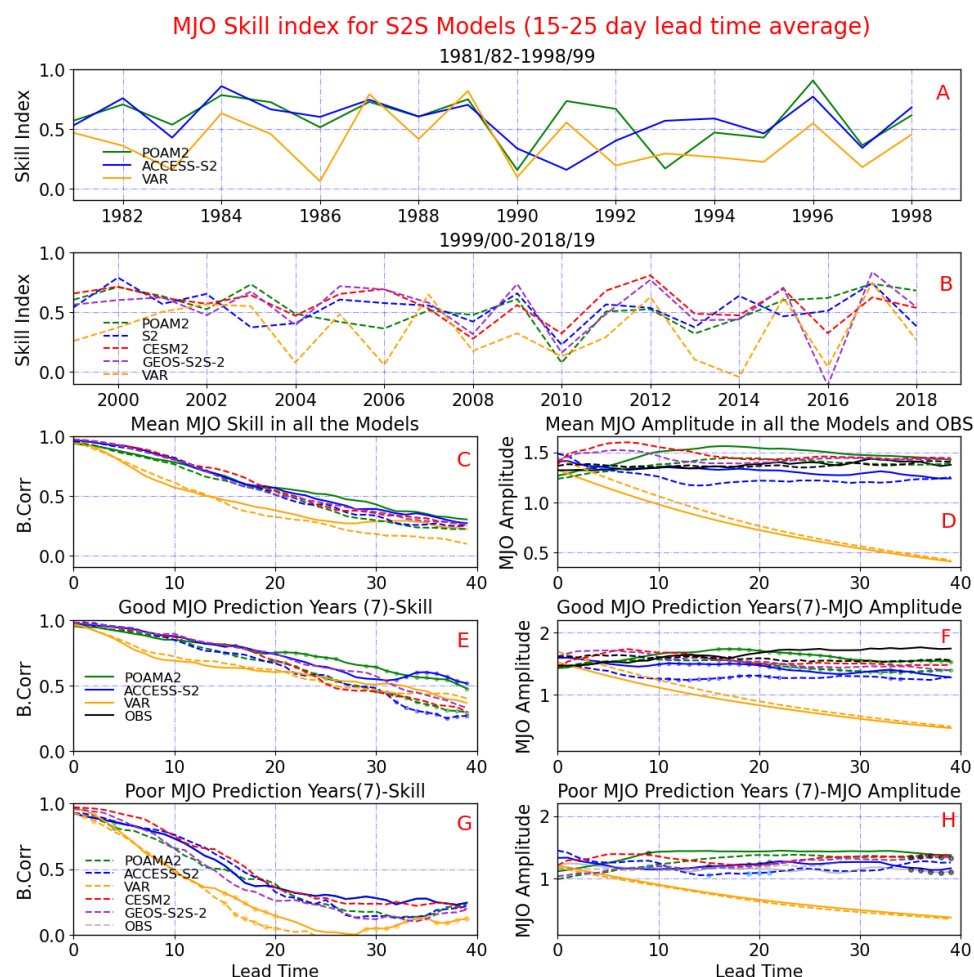


Figure 2: Comparison of MJO forecast skill metrics between 1981–1998 (solid lines) and 1999–2018 (dashed lines). (A, B) Skill indices at 15–25-day lead times across models (VAR, POAMA2, ACCESS-S2 in 1981–1998; CESM2 and GEOS-S2S-2 added in 1999–2018). (C, D) Composite mean skill and amplitude versus lead time. (E, F) Results for the seven highest-skill years (good MJO prediction); (G, H) the seven lowest-skill years (poor prediction years). Dots indicate statistically significant differences ($p < 0.05$) between periods for models present in both eras (ACCESS-S2, POAMA2, VAR). The comparison of good and poor MJO prediction years for the observed MJO amplitude is obtained using the multi-model mean skill index of the dynamical models for each period.

3.3 Mean State Biases in the Models

Figure 3 illustrates model mean state-specific humidity at 850 hPa and SST biases in the MJO forecast models across both study periods. All models exhibit an El Niño-like warming pattern in the eastern tropical Pacific, with POAMA2 and CESM2 showing the most substantial biases (exceeding $+1.5^{\circ}\text{C}$) and ACCESS-S2 showing the weakest bias ($< +0.8^{\circ}\text{C}$). The second period



(1999–2018) exhibits notable Indian Ocean warming in CESM2 and GEOS-S2S-2, contrasting with the first period (1981–1998), during which POAMA2 and ACCESS-S2 display more localised eastern Indian Ocean warming, accompanied by a characteristic negative IOD-like pattern. The identified SST biases likely affect MJO skill by modifying the background state through which the MJO propagates. The El Niño-like eastern Pacific warming may weaken the Walker circulation, and this weakening can, in turn, promote stronger eastward propagation of the MJO (Wang & Li, 2021). In the first period, negative IOD-like patterns in POAMA2/ACCESS-S2 could promote more realistic MJO initiation in phases 3 and 4.

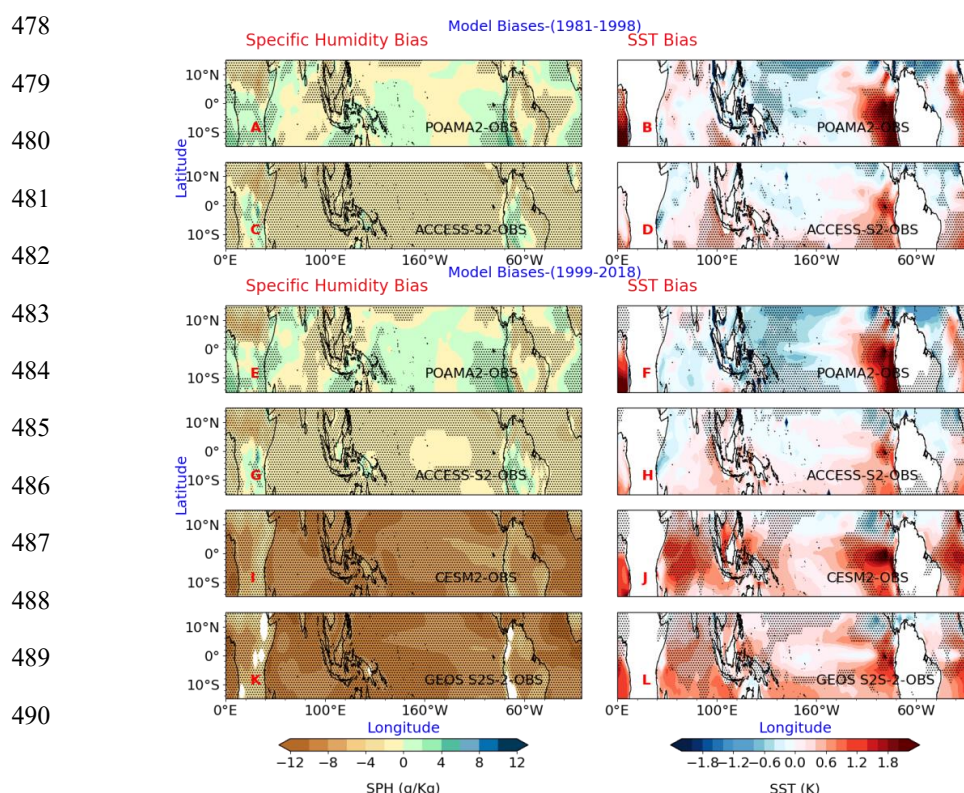


Figure 3: Mean state biases in MJO forecast models for 40-day lead time from the initialisation dates, showing differences between modelled and observed climatologies for (left) specific humidity at 850 hPa and (right) SST. Top panels (A–D) display biases for 1981–1998 from the model ensemble (POAMA2, ACCESS-S2), while bottom panels (E–L) show 1999–2018 results, including models (CESM2, GEOS-S2S-2). Positive values indicate that the model overestimates the value of the variable relative to the observations. The stippling in the figure suggests significant biases estimated using the bootstrapping method.

Inter-model and period comparisons reveal no relationship between dry biases and MJO forecast skill. While POAMA2 and ACCESS-S2 maintain consistently weaker dry biases than CESM2 and GEOS-S2S-2, their skill characteristics show period-dependent behaviour: both models achieve superior performance during high-skill years in the first period (1981–1998; Fig. 2E) but experience notable skill reduction in the second period (1999–2018) without



503 corresponding increases in moisture bias. Crucially, mean skill levels remain comparable
504 across all models despite their divergent dry bias magnitudes (e.g., CESM2/GEOS-S2S-2 vs.
505 POAMA2). This apparent disconnect suggests that moisture biases alone are insufficient to
506 explain variations in MJO forecast skill. Supporting this, Figure 3 shows positive SST biases
507 over the Maritime Continent and eastern Indian Ocean in some models that do not translate
508 into corresponding positive moisture anomalies at 850 hPa. This mismatch points to a possible
509 decoupling between SST anomalies and moisture–convection feedback, potentially linked to
510 weak surface wind anomalies or limitations in convection parameterisation. Thus, while dry
511 biases do not directly correlate with skill differences, improving convection schemes and their
512 coupling with large-scale dynamics could still be beneficial for enhancing MJO skill (Zhu &
513 Hendon, 2015), particularly during periods of weak external forcing. We investigate the
514 influence of large-scale dynamics in the following section.

515 **3.4 Large-scale dynamics influencing MJO skill in the models**

516 Figure 4 elucidates the large-scale atmospheric controls on MJO forecast skill by analysing
517 regression patterns between model and observed state variables and the MJO skill index
518 computed for individual models for respective periods. 30-day lead OLR and 850 hPa specific
519 humidity anomalies are regressed onto the MJO skill index (see Section 3.2). This approach
520 identifies characteristic patterns associated with high-skill/low-skill MJO prediction years
521 while enabling direct model-observation comparisons.

522 During the first period (1981–1998; Fig. 4, top panels), POAMA2, ACCESS-S2, and VAR
523 simulate a negative IOD-like pattern in the Indian Ocean, marked by lower-tropospheric
524 moistening in the eastern Indian Ocean (EIO) and drying in the western Indian Ocean (WIO),
525 alongside collocated OLR anomalies showing enhanced EIO convection and WIO suppression.
526 This dipole structure suggests that higher MJO skill coincides with a background state
527 replicating an IOD-driven moisture-convection feedback. In the Pacific, models exhibit weak
528 La Niña-like signatures in humidity and OLR, although these are statistically insignificant ($p >$
529 0.10). ACCESS-S2 shows the strongest La Niña signal, while VAR captures only marginal Pacific
530 anomalies. Collectively, these patterns indicate that first-period MJO skill is optimised when
531 models simulate (1) a negative IOD-like regime in the Indian Ocean, enhancing moisture
532 convergence, and (2) weak La Niña-like Pacific Ocean conditions, supporting a stronger
533 Walker circulation.

534

535

536

537

538

539

540

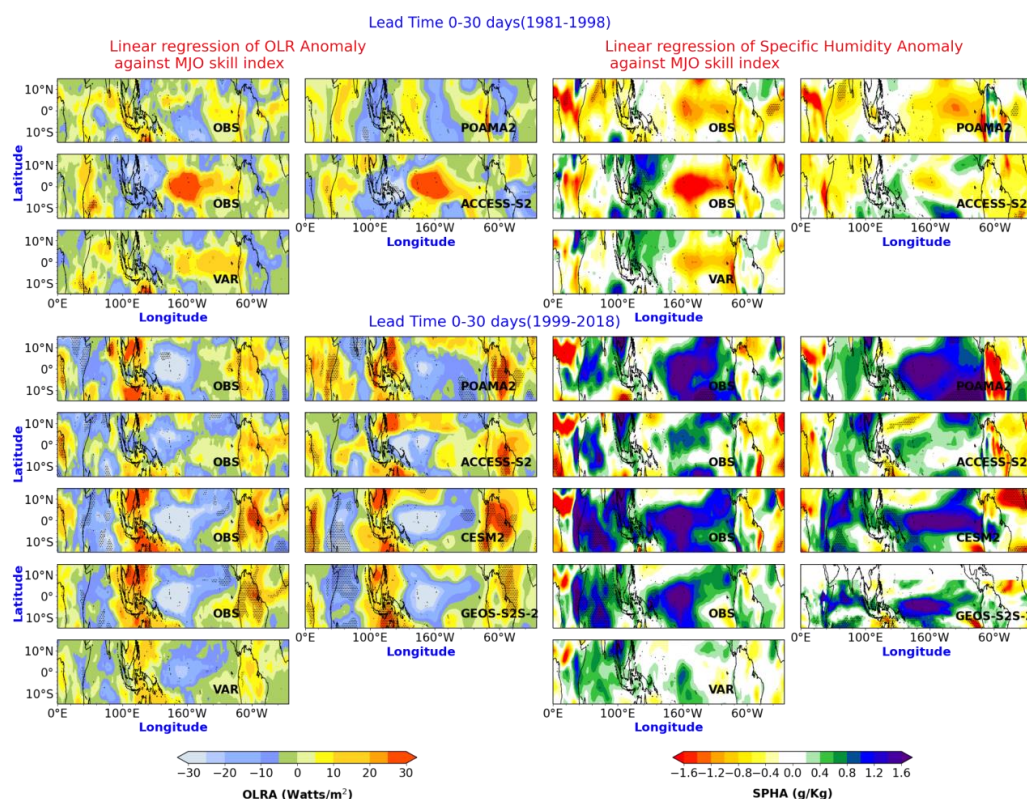


Figure 4: Linear regression of OLR anomalies and 850 hPa specific humidity anomalies onto MJO skill indices computed for individual models and periods. The top panels display results for the period from 1981 to 1998, while the bottom panels show results for the period from 1999 to 2018. Stippling marks regions where regression coefficients are statistically significant ($p < 0.10$).

During the second period (1999–2018; Fig. 4, bottom panels), the models simulate distinct shifts in the relationships with the background states. POAMA2, CESM2, and GEOS-S2S-2 exhibit strong moistening in the central Pacific, resembling a central Pacific El Niño pattern (Ashok et al., 2007), with colocated OLR anomalies showing enhanced convection; however, these linkages remain statistically insignificant ($p > 0.10$). In contrast, ACCESS-S2 and VAR lack a clear El Niño-like signature. The Indian Ocean displays divergent model behaviours: most models (excluding POAMA2, ACCESS-S2, and VAR) align with a warm IOBM regime, marked by basin-wide moistening and convection, while POAMA2, ACCESS-S2, and VAR instead reflect a positive IOD-like dipole pattern. Notably, all models systematically underestimate the observed magnitudes of moistening in the Indian Ocean across both periods, suggesting a pervasive bias in representing moisture convergence dynamics in the Indian Ocean region. These results highlight how epochal changes in tropical climate modes differentially influence model skill, with central Pacific El Niño, warm-IOBM and positive IOD-like regimes emerging as competing controls on MJO predictability in the most recent period.



560 Our analysis reveals fundamental differences in how tropospheric background states
561 modulate MJO predictability across epochs. Between 1981 and 1998, both dynamical and
562 statistical models demonstrated higher skill under consistent background conditions—a cold
563 IOD-like pattern in the Indian Ocean, coupled with weak La Niña-like Pacific anomalies—
564 suggesting robust tropospheric control of MJO predictability. Post-1998, this coherence
565 breaks down: models diverge in their responses to background states, with POAMA2, CESM2,
566 and GEOS-S2S-2 tracking central Pacific (CP) El Niño-like conditions, while ACCESS-S2 and VAR
567 exhibit either positive IOD linkages or weak tropical Pacific connections. This reduced
568 tropospheric influence likely stems from the following:

- 569 1. Increased sensitivity to Indian Ocean warming in recent years in some models
570 (Dalpadado et al., 2021);
- 571 2. ENSO diversity, particularly increased CP El Niño events (Freund et al., 2019), which
572 alter MJO propagation pathways (Chen et al., 2015) and
- 573 3. Stratospheric dominance, as the QBO's role in MJO skill, intensifies due to the
574 absence of coherent tropospheric drivers.

575 The declining inter-model agreement further underscores that contemporary MJO prediction
576 skill may depend more on interannual variability in stratospheric processes (e.g., QBO) than
577 on the tropospheric background state. This has important implications for model
578 development.

579 To elucidate the evolving relationship between large-scale drivers and MJO predictability, we
580 computed correlations between the multi-model mean skill index and the climate mode
581 indices (averaged across dynamical models) during austral summer (December-February) for
582 each period separately. This analysis reveals how the MJO-climate mode linkage has changed
583 between 1981-1998 and 1999-2018, identifying which climate condition became more or less
584 influential on MJO forecast skill over time. During 1981–1998, the multi-model mean skill
585 index exhibited the strongest correlation with the QBO index ($r = -0.41$, $p < 0.01$),
586 demonstrating enhanced predictability during EQBO years, with EQBO conditions supporting
587 extended predictability windows of 25-35 days. This was complemented by weaker but
588 consistent relationships with negative phases of the ocean-atmosphere coupled modes: IOD
589 ($r = -0.36$, $p < 0.01$), ENSO ($r = -0.30$), and IOBM ($r = -0.21$), indicating that La Niña and negative
590 IOD/IOBM conditions further enhanced predictability when coincident with EQBO. These
591 correlation patterns strongly support our earlier findings that optimal MJO predictability
592 occurred during periods when negative IOD/IOBM/ENSO phases coincided with EQBO
593 conditions. This enhanced predictability primarily results from strengthened MJO convection
594 during phases 3-6, when the MJO's convective envelope interacts most strongly with the
595 Indian Ocean-western Pacific warm pool. The combined effects of (1) EQBO-induced
596 stratospheric wind modulation and (2) warmer SSTs under negative IOD/IOBM/ENSO phases
597 create favourable conditions for enhanced lower-tropospheric moisture convergence and
598 deep convection. Both observational composites (Figure S1) and model simulations confirm
599 this amplification mechanism, demonstrating more vigorous MJO activity in phases 3-6 during
600 these co-occurring climate mode conditions (not shown). Post-1998, while the QBO influence
601 strengthened further ($r = -0.46$, $p < 0.01$), its practical impact diminished as predictability
602 windows shortened to 21-26 days during EQBO years. This paradox stems from a breakdown
603 in the previously synergistic QBO-ocean-atmosphere coupling, as evidenced by reversed
604 correlations with IOD ($r = +0.34$), ENSO ($r = +0.31$), and IOBM ($r = +0.17$) and weakened phase



alignments. This reversal occurred alongside a breakdown in favourable phase alignments (QBO-tropospheric mode correlations < 0.15), leaving no coherent multiscale forcing regime.

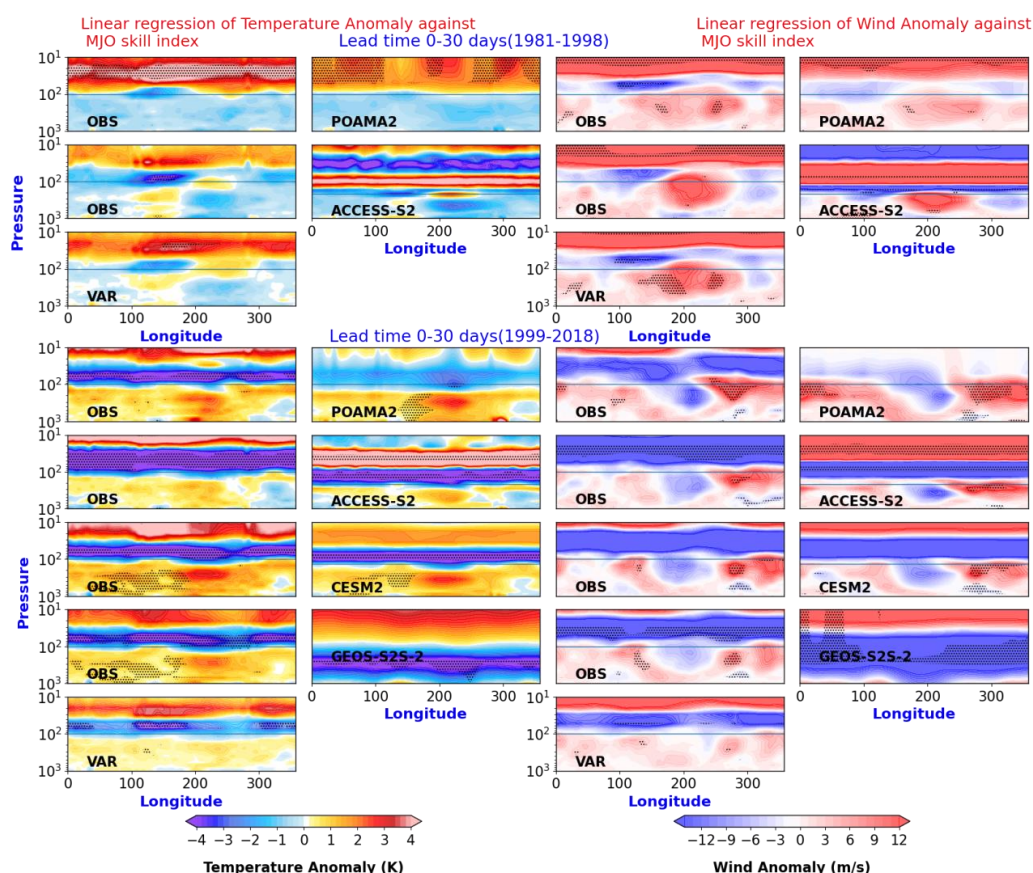


Figure 5: Linear regressions of observed and modelled vertical profiles of (a) temperature and (b) zonal wind anomalies onto each model's MJO skill index for both periods (1981-1998 and 1999-2018). The top panels present regression patterns for the earlier period (1981-1998), while the bottom panels show results for the later period (1999-2018). Stippling indicates regions where regression coefficients are statistically significant at the 90% confidence level ($p < 0.10$).

Figure 5 validates the identified MJO skill-background state relationships through vertical structure analysis, examining temperature and zonal wind anomaly profiles via linear regression with model skill indices. During 1981–1998 (top panel), all models simulate EQBO-like zonal wind patterns (easterly anomalies < 5 m/s in the lower stratosphere) which results in tropopause-level (100–200 hPa) temperature instability ($\Delta T \sim 2.2$ – 1.2 K), though with notable inter-model differences: ACCESS-S2 better resolves these stratospheric signatures compared to POAMA2, which exhibits weaker vertical coherence due to its poor stratospheric representation. These patterns intensify post-1998, with wind anomalies strengthening and temperature instability increasing by ~ 1 – 2 K, indicating enhanced QBO-MJO coupling. This



vertical structure analysis aligns with our skill-index correlations, where the QBO relationship strengthened ($r = -0.41$ to -0.46). The consistency between these independent diagnostics (regressions and correlations) demonstrates that MJO predictability has shifted from being governed by coordinated tropospheric-stratospheric drivers in the first period to increasingly stratosphere-dominated controls in the second period, with model skill strongly dependent on faithful representation of QBO-related vertical coupling processes.

3.5 Relationship Between MJO Event Characteristics in the Models and the Climate Indices

Figure 6 displays the correlation coefficients between interannual MJO characteristics in the models (mean MJO event duration and total MJO event count for every DJF) and observed climate indices. In the first period, ACCESS-S2 (compared to POAMA2 and VAR) shows a significant negative correlation (-0.48) between the QBO index and MJO event count, a stronger relationship than observed.

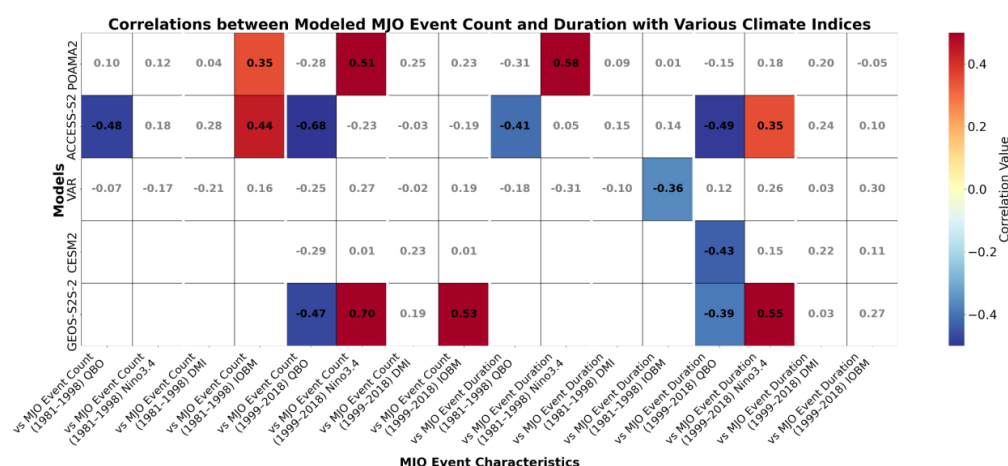


Figure 6: Correlation between MJO event characteristics (total MJO event count and mean annual event duration) against various climate indices (QBO, Niño3.4, DMI and IOBM for different periods.

In the second period, the relationship between MJO event counts and the QBO index strengthens in ACCESS-S2 (-0.68) and is also evident in GEOS-S2S-2 (-0.47). This suggests a higher MJO event count during EQBO years. This is unlike the case in the observations. Additionally, moderate negative correlations (-0.39 to -0.49) emerge between MJO event durations and QBO indices in CESM2, ACCESS-S2, and GEOS-S2S-2. However, these model-simulated relationships underestimate the observed relationships between the QBO and MJO duration linkages, except for ACCESS-S2. Because the QBO is skillfully predicted by the models (Table 2), these model-dependent relationships between the MJO characteristics and the QBO appear to originate not from stratospheric forecast errors, but from misrepresented tropospheric responses.

During the second period, both POAMA2 and GEOS-S2S-2 exhibit significant positive correlations between the Niño3.4 index and MJO event count (0.51 and 0.70, respectively),



649 in contrast to observations, which show no such relationship. This discrepancy is also evident
650 in the first period, as neither model captures the observed moderate positive MJO event
651 count-ENSO connection (see section 3.1). Additionally, these models overestimate the
652 relationship between MJO event duration and the ENSO index, suggesting that simulated MJO
653 events persist longer during El Niño years or that the models exhibit a bias toward El Niño-
654 like conditions. The El Niño-like warming bias in the Pacific Ocean region observed in Section
655 3.3 may be indicative of the same phenomenon. Klingaman and DeMott (2020) reported a
656 similar result, finding increased MJO activity during El Niño years in CMIP-class models
657 (specifically SPCAM3 and SPCCSM3), a pattern largely attributed to the East Pacific warming
658 bias present in these climate models.

659 The relationship between MJO event count and the DMI index during the first period differs
660 substantially from observations in all models except VAR. While observations indicate an
661 increase in MJO event frequency during negative IOD years, models generally fail to capture
662 this association. In the second period, some models produce weak correlations between MJO
663 event frequency and positive DMI, unlike in the observations. Notably, observations reveal
664 no significant relationship between MJO event duration and IOD phases in either period.
665 However, during the second period, most models generate weak (albeit non-significant)
666 positive correlations between MJO duration and DMI, suggesting a potential positive IOD-like
667 bias, with VAR and GEOS-S2S-2 as notable exceptions. The moderate skill in representing DMI
668 variability across models (Table 2) further implies that the fidelity of MJO-IOD linkages in
669 models may be tied to their ability to simulate IOD behaviour realistically.

670 A moderate positive correlation exists between MJO event count and the IOBM index during
671 the first period, suggesting that warm IOBM phases (W-IOBM years) are associated with
672 enhanced MJO activity in model simulations. However, observational records show no
673 significant MJO-IOBM relationship, implying this connection may be a modelling artifact
674 rather than a genuine climate feature. While Table 2 indicates that most models reproduce
675 the IOBM index with reasonable accuracy, this apparent skill in representing Indian Ocean
676 variability does not extend to the MJO-IOBM linkage, suggesting potential oversimplifications
677 or errors in the modelled physical mechanisms. During the second period, models generally
678 underestimate MJO event frequency during warm IOBM phases, with GEOS-S2S-2 being the
679 notable exception - its overestimation of this relationship may stem from the warm bias in its
680 Indian Ocean simulation (Section 3.3). Additionally, CESM2 performs distinctly worse than
681 other models in simulating IOBM-like conditions, as evidenced by its lower correlation (0.69)
682 between observed and modelled IOBM indices. The Indian Ocean warming bias identified in
683 CESM2 in Section 3.3 also supports the lower correlation.

684

685

686

687

688

689



Model	QBO	DMI	IOBM	Niño 3.4
ACCESS-S2 1981-1998	0.96	0.73	0.95	0.80
POAMA2 1981-1998	0.84	0.80	0.93	0.81
ACCESS-S2 1999-2019	0.94	0.53	0.83	0.83
POAMA2 1999-2019	0.86	0.67	0.83	0.93
CESM2	0.97	0.67	0.69	0.98
GEOS-S2S-2	0.98	0.55	0.70	0.82

Table 2: Correlations between climate mode indices computed from the observed datasets and model datasets for the two periods

4. Conclusion

Accurate prediction of the MJO is crucial for advancing S2S forecasting capabilities, given its global impact on tropical convection and extratropical teleconnections (Vitart & Robertson, 2018). Our analysis of four S2S models (POAMA2, ACCESS-S2, GEOS-S2S-2, CESM2) and a statistical benchmark (VAR) during austral summer (December–February) across two periods (1981-1998 (POAMA2, ACCESS-S2)) vs. 1999-2018 (POAMA2, ACCESS-S2, GEOS-S2S-2, CESM2)) highlights three key findings.

First, we assessed how the MJO interacts with various climate modes by conducting a composite analysis of observed MJO amplitude during different phases of the climate modes. In the earlier period, the IOD exhibited a pronounced influence on MJO amplitude, with the negative phase associated with more vigorous MJO activity. This enhancement was further supported by increased MJO amplitude during EQBO years and cold phases of the IOBM. However, in the later period, the relationship between the negative phase of the IOD and MJO amplitude disappears, leaving the MJO modulation primarily associated with the EQBO.

Additionally, during the first period, EQBO–MJO events tended to coincide with favourable tropospheric states, such as negative IOD, cold IOBM, or La Niña-like conditions, suggesting a coherent multi-mode influence. By contrast, in the second period, the connection between stratospheric and tropospheric climate modes is diminished, and QBO–MJO events occur largely independently of favourable tropospheric forcings. The annual count of MJO events in observations shows a moderate correlation with coupled ocean–atmosphere modes, while the mean yearly event duration correlates directly with EQBO conditions.

In the second part of our study, we analysed the relationship between MJO prediction skill and large-scale climate modes to verify the characteristics identified in observational records. The mean prediction skill for the MJO in ACCESS-S2 and POAMA2 showed minimal difference



716 between the two periods examined. This difference between the periods, however, is not
717 observed in the years with poor MJO predictions. The elevated skill observed in the high-skill
718 years of the first (earlier) period was primarily linked to higher MJO amplitude. These years
719 showed a clear association with EQBO-like signatures in the stratosphere, a negative IOD-like
720 pattern or cold IOBM-like pattern in the Indian Ocean sector, and, to a lesser extent, La Niña-
721 like conditions in the Pacific. This phase alignment among the stratospheric process,
722 processes in the Indian and the Pacific Oceans provided a favourable multiscale environment
723 that enhanced both MJO amplitude and model predictability. By contrast, in the second (later)
724 period, high-skill MJO years exhibited distinctly different background conditions. For these
725 years, Indian Ocean SST patterns resembled warm IOD/IOBM-like modes, and the Pacific
726 showed El Niño-like features—conditions less conducive to amplified MJO activity. As a
727 result, the previously robust synergistic connection between different climate modes
728 appeared to break down, resulting in diminished MJO predictability even in otherwise “high-
729 skill” years. Notably, EQBO remained the only significant and persistent modulator of MJO
730 skill in the second period, but its overall impact was weaker without concurrent favourable
731 patterns in other climate modes.

732 We speculate that in the later period, the weaker QBO–MJO relationship in model forecasts—
733 despite the QBO being reasonably well represented in both high-top (ACCESS-S2, GEOS-S2S-
734 2) and low-top (POAMA2) models, and consistent with the earlier period—likely reflects
735 changes in the tropospheric background state. In the second period, the models struggle to
736 capture the stratosphere–troposphere coupling, particularly in the absence of strong external
737 forcing, as was more commonly observed during the first period. Additionally, key processes
738 in the troposphere are often poorly captured by the models. For example, models analysed
739 in this study fail to accurately replicate the observed relationship between MJO event
740 frequency and duration and the ENSO index. This limitation suggests an underlying Pacific
741 bias, with many models skewing toward El Niño-like conditions, potentially linked to a known
742 warm bias in the eastern Pacific. Moreover, models (notably POAMA2, CESM2, and GEOS-
743 S2S-2) exhibit a tendency toward the warm phases of the IOD and IOBM, in contrast to
744 observed variability. These systematic biases in representing coupled ocean–atmosphere
745 background states may limit the models’ ability to simulate realistic MJO behaviour.
746 Therefore, future modelling efforts would benefit from improving the representation of
747 tropospheric circulation patterns and reducing SST-related biases, particularly in the Indo-
748 Pacific region, alongside enhanced stratospheric resolution. Such improvements may provide
749 a pathway to improving MJO prediction skill, especially during periods lacking strong
750 multiscale external forcing. A key limitation of this study is the relatively short hindcast record
751 available, particularly for some models, which constrains the ability to robustly assess longer-
752 term variability and low-frequency influences. Extending forecast datasets further back in
753 time would strengthen the ability to disentangle model biases from genuine dynamical shifts
754 and provide a more comprehensive understanding of decadal changes in MJO predictability.

755 **Code and data availability**

756 The model data analysed during this study are available from the corresponding author upon
757 reasonable request. All publicly available observational and reanalysis datasets are provided
758 by the NOAA Physical Sciences Laboratory (PSL) and the Australian Bureau of Meteorology
759 (BOM) as follows:



- 760 • The NCEP-DOE Reanalysis 2 data:
761 <https://psl.noaa.gov/data/gridded/data.ncep.reanalysis2.html>
762 • The High-Resolution OISST Version 2 data:
763 <https://psl.noaa.gov/data/gridded/data.noaa.oisst.v2.highres.html>
764 • The Real-time Multivariate MJO (RMM) index (Wheeler and Hendon, 2004):
765 <http://www.bom.gov.au/climate/mjo/graphics/rmm.74toRealtime.txt>
766 The analysis codes and scripts used in this study are available from the
767 corresponding author upon reasonable request.

768 **Supplement link**

769 **Author contributions**

770 R.R. conducted the formal analysis and led the original manuscript preparation. J.M., E.L.,
771 M.M., and J.R. provided supervision, critical guidance, and feedback. All authors contributed
772 to the study's design, interpretation of results, and manuscript review.
773

774 **Competing interests**

775
776 The contact author has declared that none of the authors has any competing interests.
777

778 **Acknowledgements**

779 The numerical analysis was conducted using Python (version 3.9). We acknowledge the
780 National Computational Infrastructure (NCI), supported by the Australian Government, for
781 providing computational resources and services. We thank the NOAA Physical Sciences
782 Laboratory for producing and making the NCEP-DOE Reanalysis II dataset publicly available.
783 We are also grateful to Drs Zoe Gillett and Hongyan Zhu at the Bureau of Meteorology for their
784 valuable feedback.

785 **Financial support**

786 This work was supported by Securing Antarctica's Environmental Future, funded by the
787 Australian Research Council (ARC) Special Research Initiative in Excellence in Antarctic Science
788 Grant SR200100005. E.L. received partial support from the Victorian Water and Climate
789 Initiative (VicWaCI) phase 2 and the National Environmental Science Program (NESP) phase 2.



790 References

- 791 • Abhik, S., & Hendon, H. H. (2019). Influence of the QBO on the MJO during coupled
792 model multiweek forecasts. *Geophysical Research Letters*, 46(15), 9213–9221.
793 <https://doi.org/10.1029/2019gl083152>
- 794 • Abhik, S., Zhang, C., & Hendon, H. H. (2023). The Indo-Pacific Maritime Continent
795 barrier effect on MJO ensemble prediction. *Geophysical Research Letters*, 50,
796 e2023GL105462. <https://doi.org/10.1029/2023GL105462>
- 797 • Cai, W., van Rensch, P., Cowan, T., & Hendon, H. H. (2011). Teleconnection pathways
798 of ENSO and the IOD and the mechanisms for impacts on Australian rainfall. *Journal*
799 *of Climate*, 24(15), 3910–3923. <https://doi.org/10.1175/2011jcli4129.1>
- 800 • Chen, Xiong & Ling, Jian & Li, Chongyin. (2015). Evolution of Madden-Julian
801 Oscillation in two types of El Niño. *Journal of Climate*. 29. 151229065042007.
802 10.1175/JCLI-D-15-0486.1.
- 803 • Cottrill, A., Hendon, H. H., Lim, E., Langford, S., Shelton, K., Charles, A., McClymont,
804 D., Jones, D., & Kuleshov, Y. (2013). Seasonal Forecasting in the Pacific Using the
805 Coupled Model POAMA-2. *Weather and Forecasting*, 28(3), 668-
806 680. <https://doi.org/10.1175/WAF-D-12-00072.1>
- 807 • Dalpadado, P., Arrigo, K. R., van Dijken, G. L., Gunasekara, S. S., Ostrowski,
808 M., Bianchi, G., & Sperfeld, E. (2021). Warming of the Indian Ocean and its impact on
809 temporal and spatial dynamics of primary production. *Progress in*
810 *Oceanography*, 198, 102688. <https://doi.org/10.1016/j.pocean.2021.102688>
- 811 • DeMott, C. A., Wolding, B. O., Maloney, E. D., & Randall, D.A. (2018). Atmospheric
812 mechanisms for MJO decay over the Maritime Continent. *Journal of Geophysical*
813 *Research: Atmospheres*, 123(10), 5188–5204.
814 <https://doi.org/10.1029/2017JD027411>
- 815 • Freund, M.B., Henley, B.J., Karoly, D.J. *et al.* Higher frequency of Central Pacific El
816 Niño events in recent decades relative to past centuries. *Nat. Geosci.* 12, 450–455
817 (2019). <https://doi.org/10.1038/s41561-019-0353-3>
- 818 • Gonzalez, A. O., and X. Jiang (2017), Winter mean lower tropospheric moisture over
819 the Maritime Continent as a climate model diagnostic metric for the propagation of
820 the Madden-Julian oscillation, *Geophys. Res. Lett.*, 44, 2588–2596,
821 doi:10.1002/2016GL072430.
- 822 • Hendon, H. H., & Abhik, S. (2018). Differences in vertical structure of the Madden-
823 Julian oscillation associated with the quasi-biennial oscillation. *Geophysical Research*
824 *Letters*, 45(9), 4419–4428. <https://doi.org/10.1029/2018GL077207>
- 825 • Huang, B., C. Liu, V. Banzon, E. Freeman, G. Graham, B. Hankins, T. Smith, and H.-M.
826 Zhang, 2021: Improvements of the Daily Optimum Interpolation Sea Surface
827 Temperature (DOISST) Version 2.1, *Journal of Climate*, 34, 2923–2939. doi:
828 10.1175/JCLI-D-20-0166.1
- 829 • Jiang, X., Adames, Á. F., Kim, D., Maloney, E. D., Lin, H., Kim, H., Waliser, D. E.,
830 Sperber, K. R., Zhang, C., & Ahn, M.-S. (2020). Fifty years of research on the Madden-
831 Julian Oscillation: Recent progress, challenges, and perspectives. *Journal of*
832 *Geophysical Research: Atmospheres*, 125(15), e2019JD030911.
833 <https://doi.org/10.1029/2019JD030911>
- 834 • Jin, D., Kim, D., Son, SW. *et al.* QBO deepens MJO convection. *Nat Commun* 14, 4088
835 (2023). <https://doi.org/10.1038/s41467-023-39465-7>



- 836 • Kanamitsu, M., Ebisuzaki, W., Woollen, J., Yang, S.-K., Hnilo, J. J., Fiorino, M., &
837 Potter, G. L. (2002). NCEP-DOE AMIP-II reanalysis (R-2). *Bulletin of the American*
838 *Meteorological Society*, 83(11), 1631–1643. [https://doi.org/10.1175/BAMS-83-11-](https://doi.org/10.1175/BAMS-83-11-163)
839 [163](https://doi.org/10.1175/BAMS-83-11-163)
- 840 • Kim, D., Xavier, P., Maloney, E., Wheeler, M., Waliser, D., Sperber, K., Hendon, H.,
841 Zhang, C., Neale, R., Hwang, Y., & Liu, H. (2014). Process-Oriented MJO
842 Simulation Diagnostic: Moisture Sensitivity of Simulated Convection. *Journal of*
843 *Climate*, 27(14), 5379–5395. <https://doi.org/10.1175/JCLI-D-13-00497.1>
- 844 • Kim, H., Janiga, M. A., & Pegion, K. (2019a). MJO propagation processes and mean
845 biases in the SubX and S2S reforecasts. *Journal of Geophysical Research:*
846 *Atmospheres*, 124, 9314–9331. <https://doi.org/10.1029/2019JD031139>
- 847 • Kim, H., Richter, J. H., & Martin, Z. (2019b). Insignificant QBO-MJO prediction skill
848 relationship in the SubX and S2S subseasonal reforecasts. *Journal of Geophysical*
849 *Research: Atmospheres*, 124, 12655–12666. <https://doi.org/10.1029/2019JD031416>
- 850 • Kim, H., Lee, M., Kim, D., Kang, H., & Hyun, Y. (2018). Representation of Boreal
851 Winter MJO and Its Teleconnection in a Dynamical Ensemble Seasonal Prediction
852 System. *Journal of Climate*, 31(21), 8803–8818. [https://doi.org/10.1175/JCLI-D-18-](https://doi.org/10.1175/JCLI-D-18-0039.1)
853 [0039.1](https://doi.org/10.1175/JCLI-D-18-0039.1)
- 854 • Klingaman, N. P., & Demott, C. A. (2020). Mean-state biases and interannual
855 variability affect perceived sensitivities of the Madden–Julian oscillation to air–sea
856 coupling. *Journal of Advances in Modeling Earth Systems*, 12, e2019MS001799.
857 <https://doi.org/10.1029/2019MS001799>
- 858 • Klotzbach, P. J., Abhik, S., Hendon, H. H., & Schreck, C. J. (2019). On the emerging
859 relationship between the stratospheric Quasi-Biennial oscillation and the Madden-
860 Julian oscillation. *Scientific Reports*, 9, 2981. [https://doi.org/10.1038/s41598-019-](https://doi.org/10.1038/s41598-019-40034-6)
861 [40034-6](https://doi.org/10.1038/s41598-019-40034-6)
- 862 • Kug, J.-S. & Sooraj, K. & Jin, Fei-Fei & Luo, Jing-Jia & Kwon, Minho. (2009). Impact of
863 Indian Ocean Dipole on high-frequency variability over the Indian Ocean.
864 *Atmospheric Research - ATMOS RES.* 94. 134–139. [10.1016/j.atmosres.2008.10.022](https://doi.org/10.1016/j.atmosres.2008.10.022).
- 865 • Liebmann, B., & Smith, C. A. (1996). Description of a complete (interpolated)
866 outgoing longwave radiation dataset. *Bulletin of the American Meteorological*
867 *Society*, 77(6), 1275–1277.
- 868 • Lim, E.-P., and Coauthors, 2021a: Why Australia was not wet during spring 2020
869 despite La Niña. *Sci. Rep.*, 11, 18423, <https://doi.org/10.1038/s41598-021-97690-w>.
- 870 • Lim, Y.-K., Arnold, N. P., Molod, A. M., & Pawson, S. (2021b). Seasonality in
871 prediction skill of the Madden-Julian Oscillation and associated dynamics in Version
872 2 of NASA's GEOS-S2S forecast system. *Journal of Geophysical Research:*
873 *Atmospheres*, 126, e2021JD034961. <https://doi.org/10.1029/2021JD034961>
- 874 • Lim, Y., Son, S.-W., & Kim, D. (2018). MJO prediction skill of the subseasonal-to-
875 seasonal prediction models. *Journal of Climate*, 31(10), 4075–4094.
876 <https://doi.org/10.1175/JCLI-D-17-0545.1>
- 877 • Lim, EP., Hendon, H.H., Zhao, M. *et al.* Inter-decadal variations in the linkages
878 between ENSO, the IOD and south-eastern Australian springtime rainfall in the past
879 30 years. *Clim Dyn* 49, 97–112 (2017). <https://doi.org/10.1007/s00382-016-3328-8>
- 880 • Ling, J., Zhao, Y., & Chen, G. (2019). Barrier Effect on MJO Propagation by the
881 Maritime Continent in the MJO Task Force/GEWEX Atmospheric System Study



- 882 Models. *Journal of Climate*, 32(17), 5529–5547. [https://doi.org/10.1175/JCLI-D-18-](https://doi.org/10.1175/JCLI-D-18-0870.1)
883 [0870.1](https://doi.org/10.1175/JCLI-D-18-0870.1)
- 884 • Lin, Q.-J., Mayta, V. C., & Adames Corraliza, Á. F. (2024). Assessment of the Madden-
885 Julian Oscillation in CMIP6 models based on moisture mode theory. *Geophysical*
886 *Research Letters*, 51, e2023GL106693. <https://doi.org/10.1029/2023GL106693>
 - 887 • Liu, X., Wu, T., Yang, S. *et al.* MJO prediction using the sub-seasonal to seasonal
888 forecast model of Beijing Climate Center. *Clim Dyn* 48, 3283–3307 (2017).
889 <https://doi.org/10.1007/s00382-016-3264-7>
 - 890 • Madden, R. A. , and P. R. Julian , 1971: Detection of a 40–50 day
891 oscillation in the zonal wind in the tropical Pacific. *J. Atmos. Sci.* , 28, 702–708,
892 [https://doi.org/10.1175/1520-0469\(1971\)028,0702:DOADOI.2.0.CO;2](https://doi.org/10.1175/1520-0469(1971)028,0702:DOADOI.2.0.CO;2).
 - 893 • Madden, R. A. , and P. R. Julian , 1972: Description of global-scale circulation cells in
894 the tropics with a 40–50 day period. *J. Atmos. Sci.* , 29, 1109–1123,
895 [https://doi.org/10.1175/1520-0469\(1972\)029,1109:DOGCC.2.0.CO;2](https://doi.org/10.1175/1520-0469(1972)029,1109:DOGCC.2.0.CO;2).
 - 896 • Maharaj, E. A., & Wheeler, M. C. (2005). Forecasting an index of the Madden-
897 oscillation. *International Journal of Climatology*, 25, 1611–1618.
 - 898 • Marshall, A. G., Hendon, H. H., Son, S. W., & Lim, Y. (2017). Impact of the quasi-
899 biennial oscillation on predictability of the Madden–Julian oscillation. *Climate*
900 *Dynamics*, 49(4), 1365–1377. <https://doi.org/10.1007/s00382-016-3392-0>
 - 901 • Martin, Z., Orbe, C., Wang, S., & Sobel, A. (2021). The MJO–QBO relationship in a
902 GCM with stratospheric nudging. *Journal of Climate*, 34(11), 4603–4624.
903 <https://doi.org/10.1175/JCLI-D-20-0636.1>
 - 904 • Mengist, C. K., & Seo, K.-H. (2022). How long can the MJO be predicted during the
905 combined phases of ENSO and QBO? *Geophysical Research Letters*, 49,
906 e2022GL097752. <https://doi.org/10.1029/2022GL097752>
 - 907 • Molod, A., Hackert, E., Vikhliayev, Y., Zhao, B., Barahona, D., Vernieres, G., et al.
908 (2020). GEOS-S2S Version 2: The GMAO high-resolution coupled model and
909 assimilation system for seasonal prediction. *Journal of Geophysical Research:*
910 *Atmospheres*, 125, e2019JD031767. <https://doi.org/10.1029/2019JD031767>
 - 911 • Neena, J. M., Lee, J. Y., Waliser, D., Wang, B., & Jiang, X. (2014). Predictability of the
912 Madden–Julian oscillation in the Intraseasonal Variability Hindcast Experiment
913 (ISVHE). *Journal of Climate*, 27(12), 4531–4543. [https://doi.org/10.1175/JCLI-D-13-](https://doi.org/10.1175/JCLI-D-13-00624.1)
914 [00624.1](https://doi.org/10.1175/JCLI-D-13-00624.1)
 - 915 • Nishimoto, E., & Yoden, S. (2017). Influence of the stratospheric quasi-biennial
916 oscillation on the Madden–Julian Oscillation during austral summer. *Journal of the*
917 *Atmospheric Sciences*, 74(4), 1105–1125. <https://doi.org/10.1175/JAS-D-16-0205.1>
 - 918 • Peatman, S.C., Matthews, A.J. and Stevens, D.P. (2014), Propagation of the Madden–
919 Julian Oscillation through the Maritime Continent and scale interaction with the
920 diurnal cycle of precipitation. *Q.J.R. Meteorol. Soc.*, 140: 814–825.
921 <https://doi.org/10.1002/qj.2161>
 - 922 • Pegion, K., Kirtman, B. P., Becker, E., Collins, D. C., LaJoie, E., Burgman, R., Bell, R.,
923 DelSole, T., Min, D., Zhu, Y., Li, W., Sinsky, E., Guan, H., Gottschalck, J., Metzger, E. J.,
924 Barton, N. P., Achuthavarier, D., Marshak, J., Koster, R. D., Lin, H., Gagnon, N., Bell,
925 M., Tippett, M. K., Robertson, A. W., Sun, S., Benjamin, S. G., Green, B. W., Bleck, R.,
926 & Kim, H. (2019). The Subseasonal Experiment (SubX): A multi-model subseasonal
927 prediction experiment. *Bulletin of the American Meteorological Society*.
928 <https://doi.org/10.1175/BAMS-D-18-0270.1>



- 929 • Rashid, H. A., Hendon, H. H., Wheeler, M. C., & Alves, O. (2011). Prediction of the
930 Madden–Julian oscillation with the POAMA dynamical prediction system. *Climate*
931 *Dynamics*, 36(3), 649–661. <https://doi.org/10.1007/s00382-010-0754-x>
- 932 • Richter, J. H., & Coauthors. (2022). Subseasonal Earth system prediction with CESM2.
933 Weather and Forecasting, 37, 797–815. <https://doi.org/10.1175/WAF-D-21-0163.1>
- 934 • Roy, R., Arblaster, J. M., Wheeler, M. C., & Lim, E.-P. (2025). Understanding MJO
935 teleconnections to the Southern Hemisphere extratropics during El Niño, La Niña,
936 and neutral years. *Geophysical Research Letters*, 52, e2024GL113395.
937 <https://doi.org/10.1029/2024GL113395>.
- 938 • Saji, N. H., Goswami, B. N., Vinayachandran, P. N., & Yamagata, T. (1999). A dipole
939 mode in the tropical Indian Ocean. *Nature*, 401, 360–363.
- 940 • Sakaeda, N., Dias, J., & Kiladis, G. N. (2020). The unique characteristics and potential
941 mechanisms of the MJO-QBO relationship. *Journal of Geophysical Research:*
942 *Atmospheres*, 125, e2020JD033196. <https://doi.org/10.1029/2020JD033196>
- 943 • Savarin, A., & Chen, S. S. (2023). Land-locked convection as a barrier to MJO
944 propagation across the Maritime Continent. *Journal of Advances in Modeling Earth*
945 *Systems*, 15, e2022MS003503. <https://doi.org/10.1029/2022MS003503>
- 946 • Schott, F. A., Xie, S.-P., & McCreary, J. (2009). Indian Ocean circulation and climate
947 variability. *Reviews of Geophysics*, 47(1). <https://doi.org/10.1029/2007rg000245>
- 948 • Son, S. W., Lim, Y., Yoo, C., Hendon, H. H., & Kim, J. (2017). Stratospheric control of
949 the Madden–Julian Oscillation. *Journal of Climate*, 30(6), 1909–1922.
950 <https://doi.org/10.1175/JCLI-D-16-0620.1>
- 951 • Stan, C., Zheng, C., Chang, E. K., Domeisen, D. I. V., Garfinkel, C. I., Jenney, A. M., Kim,
952 H., Lim, Y., Lin, H., Robertson, A., Schwartz, C., Vitart, F., Wang, J., & Yadav, P. (2022).
953 Advances in the Prediction of MJO Teleconnections in the S2S Forecast Systems.
954 *Bulletin of the American Meteorological Society*, 103(6), E1426–E1447.
955 <https://doi.org/10.1175/BAMS-D-21-0130.1>
- 956 • Sun, L., Wang, H., & Liu, F. (2019). Combined effect of the QBO and ENSO on the
957 MJO. *Atmospheric and Oceanic Science Letters*, 12(3), 170–176.
958 <https://doi.org/10.1080/16742834.2019.1588064>
- 959 • Trenberth, K. E. (1997). The Definition of El Niño. *Bulletin of the American*
960 *Meteorological Society*, 78(12), 2771–2778.
- 961 • Tseng, K.-C., Barnes, E. A., & Maloney, E. D. (2018). Prediction of the midlatitude
962 response to strong Madden-Julian oscillation events on S2S time scales. *Geophysical*
963 *Research Letters*, 45, 463–470. <https://doi.org/10.1002/2017GL075734>
- 964 • Vitart, F., 2017: Madden–Julian oscillation prediction and teleconnections in the S2S
965 database. *Quart. J. Roy. Meteor. Soc.*, 143, 2210–2220,
966 <https://doi.org/10.1002/qj.3079>.
- 967 • Vitart, F., Robertson, A.W. The sub-seasonal to seasonal prediction project (S2S) and
968 the prediction of extreme events. *npj Clim Atmos Sci* 1, 3 (2018).
969 <https://doi.org/10.1038/s41612-018-0013-0>
- 970 • Wedd R, Alves O, de Burgh-Day C, Down C, Griffiths M, Hendon HH, Hudson D, Li S,
971 Lim EP, Marshall AG, Shi L (2022) ACCESS-S2: the upgraded bureau of meteorology
972 multi-week to seasonal prediction system. *J South Hemisph Earth Syst Sci*.
973 <https://doi.org/10.1071/ES22026>



- 974 • Wei, Y., & Ren, H. (2019). Modulation of ENSO on Fast and Slow MJO Modes during
975 Boreal Winter. *Journal of Climate*, 32(21), 7483–7506. [https://doi.org/10.1175/JCLI-](https://doi.org/10.1175/JCLI-D-19-0013.1)
976 [D-19-0013.1](https://doi.org/10.1175/JCLI-D-19-0013.1)
977 • Wilson, E. A., A. L. Gordon, and D. Kim (2013), Observations of the Madden Julian
978 Oscillation during Indian Ocean Dipole events, *J. Geophys. Res. Atmos.*, 118, 2588–
979 2599, doi:10.1002/jgrd.50241.
980 • Wu, J., Ren, H.-L., Jia, X., & Zhang, P. (2023). Climatological diagnostics and
981 subseasonal-to-seasonal predictions of Madden–Julian Oscillation events.
982 *International Journal of Climatology*, 43(5), 2449–2464.
983 <https://doi.org/10.1002/joc.7984>
984 • Xie, S., Hu, K., Hafner, J., Tokinaga, H., Du, Y., Huang, G., & Sampe, T. (2009). Indian
985 Ocean Capacitor Effect on Indo–Western Pacific Climate during the Summer
986 following El Niño. *Journal of Climate*, 22(3), 730–747.
987 <https://doi.org/10.1175/2008JCLI2544.1>
988 • Zavadoff, B. L., Gao, K., Lopez, H., Lee, S.-K., Kim, D., & Harris, L. M. (2023). Improved
989 MJO forecasts using the experimental global-nested GFDL SHIELD model.
990 *Geophysical Research Letters*, 50, e2022GL101622.
991 <https://doi.org/10.1029/2022GL101622>
992 • Zhang, C. (2013). Madden–Julian Oscillation: Bridging Weather and Climate. *Bulletin*
993 *of the American Meteorological Society*, 94(12), 1849–1870.
994 <https://doi.org/10.1175/BAMS-D-12-00026.1>
995 • Zhang, C., & Ling, J. (2017). Barrier effect of the Indo-Pacific Maritime continent on
996 the MJO: Perspectives from tracking MJO precipitation. *Journal of Climate*, 30(9),
997 3439–3459. <https://doi.org/10.1175/jcli-d-16-0614.1>
998 • Zhao, M., Hendon, H. H., Alves, O., Liu, G., & Wang, G. (2016). Weakened Eastern
999 Pacific El Niño Predictability in the Early Twenty-First Century. *Journal of Climate*,
1000 29(18), 6805–6822. <https://doi.org/10.1175/JCLI-D-15-0876.1>
1001 • Zhou, X., Wang, L., Hsu, P., Li, T., & Xiang, B. (2024). Understanding the Factors
1002 Controlling MJO Prediction Skill across Events. *Journal of Climate*, 37(20), 5323–5336.
1003 <https://doi.org/10.1175/JCLI-D-23-0635.1>
1004 • Zhu, H. and Hendon, H.H. (2015), Role of large-scale moisture advection for
1005 simulation of the MJO with increased entrainment. *Q.J.R. Meteorol. Soc.*, 141: 2127–
1006 2136. <https://doi.org/10.1002/qj.2510>
1007 • Zu, Y., Sun, S., Fang, Y., Liu, L., Gao, L., Guo, G., & Li, J. (2024). Weakening of La Niña
1008 impact on negative Indian Ocean Dipole under global warming. *Geophysical Research*
1009 *Letters*, 51, e2024GL110039. <https://doi.org/10.1029/2024GL110039>
1010
1011